Relative Energetics of C-H and C-C Bond Activation of Alkanes: Reactions of Ni^+ and Fe^+ with Propane on the Lowest Energy (Adiabatic) Potential Energy Surfaces

Petra A. M. van Koppen,*,† Michael T. Bowers,*,† Ellen R. Fisher,‡ and P. B. Armentrout*,‡

Contribution from the Departments of Chemistry, University of California, Santa Barbara, California 93106, and University of Utah, Salt Lake City, Utah 84112

Received October 20, 1993®

Abstract: Reactions of Fe^+ and Ni^+ with propane, propane-*2*-d_1, propane-*2,2*-d_2, propane-*1,1,1*-d_3, propane-*1,1,1,3,3,3*-d_6 and propane-d_8 are examined to gain insight into the mechanism and energetics for the H_2 and CH_4 elimination channels. The questions of C-H and/or C-C bond activation and the relative contributions from primary and secondary C-H bond activation are addressed. Total cross section measurements indicate that ground-state $Ni^+(^2D)$ and $Fe^+(^6D)$ react with propane inefficiently, 13% and 7.5% of the Langevin collision cross section, respectively, with CH_4 loss favored over H_2 loss by a factor of 4.0 for Ni^+ and 2.8 for Fe^+. For reactions with C_3D_8, the total cross sections decrease by factors of 3.8 for Ni^+ and 4.4 for Fe^+ relative to C_3H_8, with the dehydrogenation channel enhanced over demethanation for both Ni^+ and Fe^+. Kinetic energy release distributions (KERDs) from nascent metastable Ni(propane)$^+$ and Fe(propane)$^+$ complexes were measured for H_2 loss and CH_4 loss. For H_2 loss, the distribution is bimodal. Studies using propane-*2,2*-d_2 and propane-*1,1,1,3,3,3*-d_6 indicate that both primary and secondary C-H insertions are involved as initial steps. Initial secondary C-H insertion is responsible for the high-energy component in the bimodal KERD, which is much broader than predicted from statistical theory, indicating that a tight transition state leads to the final products. The low-energy component for H_2 loss involves initial primary C-H insertion and appears to be statistical, suggesting little or no reverse activation barrier as the system separates to products. The kinetic energy distribution for demethanation is statistical and is very sensitive to the energy of the rate-limiting C-H insertion transition state. A lower limit for the energy of this transition state is obtained by modeling the experimental kinetic energy release distribution for demethanation using statistical phase space theory. The barrier reduces the contribution of high angular momentum states to the final products, thus reducing the high-energy portion of the product kinetic energy distribution. Modeling the cross section, the isotope effect, and the KERD for CH_4 loss using statistical phase space theory indicates that the barrier for C-H bond insertion is located 0.10 ± 0.03 eV below the Ni^+/C_3H_8 asymptotic energy and 0.075 ± 0.03 eV below the Fe^+/C_3H_8 ground-state asymptotic energy. All data can be explained by initial C-H insertion, without the need to invoke initial C-C bond activation for ground-state Fe^+ and Ni^+ reacting with propane at low kinetic energy.

Introduction

Studies of atomic transition-metal ions reacting with simple alkanes in the gas phase have given detailed insight into the mechanism and energetics of these reactions.[1] In particular, considerable effort has been directed at understanding the mechanism and energetics of C-H and C-C bond activation by metal ions.[2-11] In a recent study of Co^+ reacting with propane, tremendous progress was made toward the understanding of C-H and C-C bond activation in simple alkanes.[12] Co^+ reacts exothermically with propane, eliminating molecular hydrogen and methane. Propane is of particular interest because it is the smallest alkane to react at thermal energies with Co^+ via oxidative addition followed by reductive elimination. Methane and ethane lead only to adduct formation, even though H_2 loss is exothermic for Co^+ reacting with ethane. Many exoergic gas-phase ion-molecule reactions occur near the collision rate at thermal energy due to the electrostatic attraction between the ion and the neutral. In these cases the chemical activation provided by the attractive interaction is sufficient to overcome intrinsic barriers that may be associated with insertion into a C-H or C-C bond. The total cross section measurement for Co^+ reacting with propane, however, was found to be inefficient, occurring at only 13% of the collision limit.[13] For Co^+ reacting with C_3D_8, the cross section was found to be even lower, reduced by nearly a factor of 3 relative to C_3H_8. The inefficiency of the reaction and the isotope effect were quantitatively modeled by assuming a rate-limiting transition state associated with initial C-H bond activation, as shown schematically in Figure 1.

In addition to restricting the flow of reactants to products, the tight transition state depicted in Figure 1 was shown to significantly reduce the average kinetic energy released for the methane elimination channel. The kinetic energy release distribution (KERD) for an exothermic process with no reverse activation energy barrier is determined mainly by the potential

† University of California.
‡ University of Utah.
® Abstract published in *Advance ACS Abstracts*, April 1, 1994.

(1) For a recent review, see: Eller, K.; Schwarz, H. *Chem. Rev.* **1991**, *91*, 1121 and references therein.
(2) *Selective Hydrocarbon Activation: Principles and Progress*; Davies, J. A., Watson, P. L., Liebman, J. F., Greenberg, A. Eds.; VCH: New York, 1990. *Bonding Energetics in Organometallic Compounds*; Mark, T. J., Ed.; ACS Symposium Series 428; American Chemical Society: Washington, DC, 1990.
(3) Weisshaar, J. C. *Acc. Chem. Res.* **1993**, *26*, 213.
(4) Tolbert, M. A.; Beauchamp, J. L. *J. Am. Chem. Soc.* **1984**, *106*, 8117.
(5) Schultz, R. H.; Elkind, J. L.; Armentrout, P. B. *J. Am. Chem. Soc.* **1988**, *110*, 411.
(6) Tonkyn, R.; Ronan, M.; Weisshaar, J. C. *J. Phys. Chem.* **1988**, *92*, 92.
(7) Jacobson, D. B.; Freiser, B. S. *J. Am. Chem. Soc.* **1983**, *105*, 5197.
(8) Houriet, R.; Halle, L. F.; Beauchamp, J. L. *Organometallics* **1983**, *2*, 1818.
(9) Armentrout, P. B.; Beauchamp, J. L. *Acc. Chem. Res.* **1989**, *22*, 315.
(10) Armentrout, P. B. In *Gas Phase Inorganic Chemistry*; Russel, D., Ed.; Plenum: New York, 1989; p 1.
(11) (a) See: Schulze, C.; Schwarz, H.; Peake, D. A.; Gross, M. L. *J. Am. Chem. Soc.* **1987**, *109*, 2368 and references therein. (b) Schwarz, H. *Acc. Chem. Res.* **1989**, *22*, 282.
(12) van Koppen, P. A. M.; Brodbelt-Lustig, J.; Bowers, M. T.; Dearden, D. V.; Beauchamp, J. L.; Fisher, E. R.; Armentrout, P. B. *J. Am. Chem. Soc.* **1991**, *113*, 2359; **1990**, *112*, 5663.
(13) Gioumousis, G.; Stevenson, D. P. *J. Chem. Phys.* **1958**, *29*, 294.

0002-7863/94/1516-3780$04.50/0

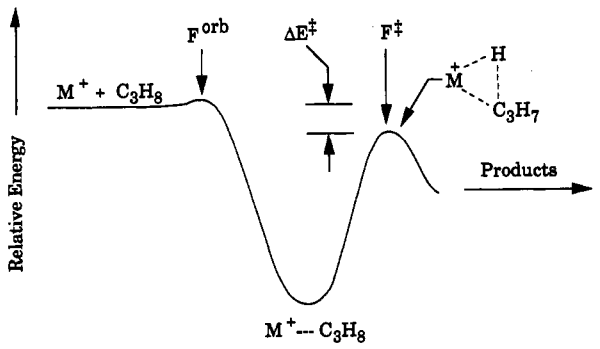

Figure 1. Schematic reaction coordinate diagram for insertion of Co^+, Fe^+, or Ni^+ into a C–H bond of C_3H_8. The fluxes through the orbiting and tight transition states are depicted as F^{orb} and $F^{\ddagger}$, respectively.

energy surface in the region of the exit channel, with the angular momentum constraints being provided by the orbiting transition state encountered during the initial interaction. More restrictive angular momentum constraints can arise, however, from a tight transition state occurring earlier along the reaction coordinate such as $F^{\ddagger}$ shown in Figure 1. It is the position and energy of this rate-limiting transition state that makes the propane system so sensitive to small perturbations such as isotope and angular momentum effects. Statistical phase space theory[14,15] was shown to successfully model the reaction cross section, the isotope effect, and the kinetic energy release distribution for demethanation of propane at thermal energies if C–H rather than C–C bond activation was assumed to be the initial rate-limiting step in the reaction. The KERD for dehydrogenation, on the other hand, indicated that both primary and secondary C–H insertion are involved as initial steps of the reaction.

In this paper, we extend the earlier Co^+ studies to Fe^+ and Ni^+. We are interested in determining if the reaction mechanisms obtained for cobalt apply to other first row transition-metal ions. Among the questions we will address in this paper is the relationship of the electronic configuration of the reactant ion ground state to its reactivity and the effect of low-lying excited states on the character of the adiabatic (reactive) potential energy surface. Cobalt ion has a ^3F, $3d^8$ ground state, while Ni^+ has a ^2D, $3d^9$ ground state.[16] The first excited states of these metal ions are $Co^+(^5F, 4s3d^7)$, 0.45 eV above the ground state, and $Ni^+(^4F, 4s3d^8)$, 1.09 eV above the ground state. In contrast, the ground state of Fe^+ is a ^6D, $4s3d^6$, and the first excited state is a ^4F, $3d^7$, only 0.25 eV higher in energy. Previous work[5,17,18] suggests that transition-metal ions in states where the 4s orbital is occupied have much weaker electrostatic interactions with neutral molecules than do states where the 4s orbital is empty. Further, these states are relatively unreactive with alkanes because occupation of the 4s orbital forces at least one of the electrons into an antibonding orbital in any insertion transition state.[5,6,19] In the cases of Co^+ and Ni^+, with low-spin, $3d^n$ ground states, these considerations suggest that the excited states should have no effect on the adiabatic reactivity of the ground-state ions with propane.

In the case of Fe^+ it appears that surfaces evolving from the ^6D, $4sd^6$ ground state and the ^4F, $3d^7$ excited state will cross. As discussed elsewhere,[5,20] the intermediates expected to be important in the reaction of Fe^+ with propane should have quartet spins, as should the products formed in the exothermic dehydrogenation and demethanation reactions.[21] Thus, the reactivity of the $Fe^+(^6D)$ ground state with propane is believed to involve a crossing to the quartet surface evolving from the $Fe^+(^4F)$ first excited state. Using this model, conclusions will be drawn about the nature and energetics of the quartet potential energy surface that leads to reductive elimination products when starting with sextet ground-state reactants. A similar but more straightforward analysis will also be made for $Ni^+(^2D)$ reacting with propane.

Experimental Section

Metastable kinetic energy release distributions were measured at UCSB using a reverse geometry double focusing mass spectrometer (VG Instruments ZAB-2F)[22] with a home-built variable temperature EI/CI source. Metal ions were formed by electron impact (150 eV) on $Fe(CO)_5$ and $Ni(CO)_6$. Typical source pressures were 10^{-3} Torr, and source temperatures were kept below 280 K to minimize decomposition of metal-containing compounds on insulating surfaces. The organometallic ions were formed in the ion source by reaction of the bare metal ions with propane. The ion source was operated at near field-free conditions to prevent kinetic excitation of ions. The ions were accelerated to 8 kV after leaving the source and mass analyzed using a magnetic sector. Metastable ions decomposing in the second field-free region between the magnetic and electric sectors were energy analyzed by scanning the electric sector. The sampled $M(propane)^+$ ions are those which decompose between 6 and 14 μs after exiting the ion source. The metastable peaks were collected with a multichannel analyzer and differentiated to yield kinetic energy release distributions.[23] Integrated peak areas were used to obtain the product distributions. The resolution of the main beam was sufficient to avoid contribution to the metastable peak widths.

The ion beam results were obtained on the Utah guided ion beam apparatus, which has been described in detail previously.[24] Ni^+ is formed by surface ionization, such that the ions are largely in their ^2D ground state (99%). A flow tube source, described in detail previously,[25] is used to generate Fe^+. Metal ions are produced by Ar ion (generated in a 1.5–3.0 keV dc discharge) sputtering of a cylindrical rod (1.25 cm in diameter and 2.5 cm in length) made of carbon steel. The ions are then swept down a 1-m-long flow tube by He and Ar flow gases maintained at pressures of 0.50 and 0.05 Torr, respectively. Under these conditions, the ions are calculated to undergo $\sim 10^5$ collisions with He and $\sim 10^4$ collisions with Ar before exiting the flow tube. Diagnostic experiments indicate that the Fe^+ beam comprises >97% ground-state ^6D ions.[26] The ions are focused into a magnetic sector for mass analysis, decelerated to a desired kinetic energy, and injected into an octopole ion guide. The octopole passes through a static gas cell, into which the reactant gas is introduced. Pressures are maintained at a sufficiently low level (<0.1 mTorr) that multiple ion–molecule collisions are improbable. Product and unreacted beam ions are contained in the guide until they leave the gas cell. The ions are then focused into a quadrupole mass filter for product mass analysis and detected by means of a scintillation ion counter. Raw ion intensities are converted to absolute cross sections as described previously.[24]

The absolute energy and the energy distribution of the reactant metal ions are measured by using the octopole as a retarding field analyzer. The fwhm of the energy distribution is generally 0.5 eV in the laboratory frame for these reactions. Uncertainties in the absolute energy scale are ±0.05 eV lab. Translational energies in the laboratory frame of reference are related to energies in the center of mass (CM) frame by $E_{CM} = E_{lab}m/(M + m)$, where M and m are the masses of the incident ion and the neutral reactant, respectively.

(14) (a) Pechukas, P.; Light, J. C.; Rankin, C. *J. Chem. Phys.* **1966**, *44*, 794. (b) Nikitin, E. *Theor. Exp. Chem. (Engl. Transl.)* **1965**, *1*, 285.
(15) (a) Chesnavich, W. J.; Bowers, M. T. *J. Am. Chem. Soc.* **1976**, *98*, 8301. (b) Chesnavich, W. J.; Bowers, M. T. *J. Chem. Phys.* **1978**, *68*, 901. (c) Chesnavich, W. J.; Bowers, M. T. *Prog. React. Kinet.* **1982**, *11*, 137.
(16) (a) Moore, C. E. *Atomic Energy Levels*; U.S. National Bureau of Standards: Washington, DC, 1952; Circ. 467. (b) Sugar, J.; Corliss, C. *J. Phys. Chem. Ref. Data* **1981**, *10*, 197, 1097. (c) Ibid. **1982**, *11*, 135.
(17) van Koppen, P. A. M.; Kemper, P. R.; Bowers, M. T. *J. Am. Chem. Soc.* **1992**, *114*, 1083. van Koppen, P. A. M.; Kemper, P. R.; Bowers, M. T. *J. Am. Chem. Soc.* **1992**, *114*, 10941.
(18) Loh, S. K.; Fisher, E. R.; Lian, L.; Schultz, R. H.; Armentrout, P. B. *J. Phys. Chem.* **1989**, *93*, 3159.
(19) (a) Armentrout, P. B. *Science* **1991**, *251*, 175. (b) Armentrout, P. B.; *Annu. Rev. Phys. Chem.* **1990**, *41*, 313.
(20) (a) Hanton, S. D.; Noll, R. J.; Weisshaar, J. C. *J. Chem. Phys.* **1992**, *96*, 5176. (b) Hanton, S. D.; Noll, R. J.; Weisshaar, J. C. *J. Phys. Chem.* **1990**, *94*, 5655.
(21) Sodupe, M.; Bauschlicher, C. W.; Langhoff, S. R.; Partridge, H. *J. Phys. Chem.* **1992**, *96*, 2118.
(22) Morgan, R. P.; Beynon, J. H.; Bateman, R. H.; Green, B. N. *Int. J. Mass Spectrom. Ion Phys.* **1978**, *28*, 171.
(23) (a) Jarrold, M. F.; Illies, A. J.; Bowers, M. T. *Chem. Phys.* **1982**, *65*, 19. (b) Kirchner, N. J.; Bowers, M. T. *J. Phys. Chem.* **1987**, *91*, 2573.
(24) Ervin, K. M.; Armentrout, P. B. *J. Chem. Phys.* **1985**, *83*, 166.
(25) Schultz, R. H.; Armentrout, P. B. *Int. J. Mass Spectrom. Ion Processes* **1991**, *121*, 121.
(26) Clemmer, D. E.; Chen, Y.-M.; Khan, F. A.; Armentrout, P. B., manuscript in preparation.

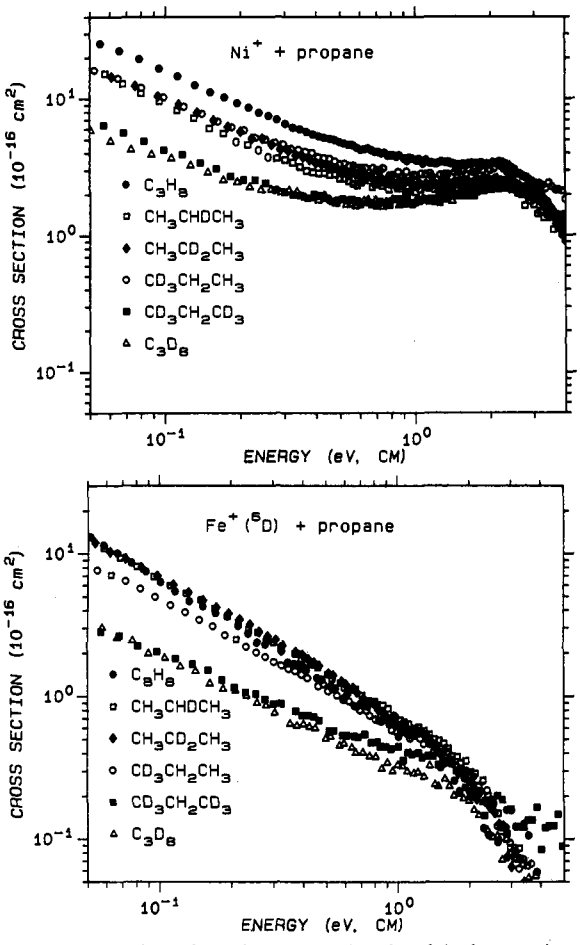

Figure 2. Variation of total cross section for dehydrogenation and demethanation as a function of kinetic energy in the center-of-mass frame for the reaction of (a, top) Ni^+ and (b, bottom) Fe^+ with propane (●), propane-*2*-d_1 (□), propane-*2,2*-d_2 (♦), propane-*1,1,1*-d_3 (◊), propane-*1,1,1,3,3,3*-d_6 (■), and propane-d_8 (△).

All compounds were obtained commercially and admitted to the mass spectrometer after several freeze–pump–thaw cycles to remove noncondensable gases. The deuterated hydrocarbons were obtained from Merck, Sharpe and Dohme. The stated minimum isotopic purities were 98% for all the labeled propanes except for $CD_3CD_2CD_3$, which was 99% pure.

Results

Absolute cross section measurements were obtained by using a guided ion beam apparatus[5,24] for reactions of Ni^+ and Fe^+ with propane, propane-*2*-d_1, propane-*2,2*-d_2, propane-*1,1,1*-d_3, propane-*1,1,1,3,3,3*-d_6, and propane-d_8. The total cross section measurements as a function of kinetic energy for Ni^+ and Fe^+ reacting with propane and the labeled propanes are shown in Figures 2a and 2b. Measurements taken at the lowest energy, 0.05 eV, are listed in Tables 1 and 2. The magnitude of the absolute cross section decreases as the extent of deuteration increases. The reaction efficiencies ($\sigma_{tot}/\sigma_{LGS}$), where σ_{LGS} is the Langevin–Gioumousis–Stevenson capture theory cross section, are very low.[13] Ni^+ reacts with C_3H_8 at 13% of the collision rate and with C_3D_8 at only 3% of the collision rate. The efficiency of Fe^+ reacting with C_3H_8 and C_3D_8 is even lower, 7.5% and 1.7% of the collision rate, respectively.

$Fe(propane)^+$ and $Ni(propane)^+$ adducts were observed more easily as the extent of deuteration increased, consistent with the concomitant increase in the density of states. The adduct lifetimes, listed in Tables 1 and 2, were obtained from the pressure dependence observed for the cross sections of these adducts[4] and calculated using statistical phase space theory.[14,15] The calculated results are in reasonable agreement with the experimental adduct lifetimes and are within the experimental time window for metastable decomposition.[27] For the C_3H_8 system, adduct formation is negligible at the pressures typically used to obtain cross section data.

Table 1. Ni^+ Reacting with Isotopically Substituted Propanes

system	total cross section (Å²)[a]	$(\sigma_{tot}/\sigma_{LGS})^b$	adduct lifetime (μs) exp[c]	adduct lifetime (μs) theory[d]
C_3H_8	25 ± 2	0.13	3.8	2.6 (+3.5/−1.4)
CH_3CHDCH_3	17 ± 2	0.09	3.3	
$CH_3CD_2CH_3$	17 ± 2	0.09	4.1	
$CH_3CH_2CD_3$	17 ± 2	0.09	9.6	
$CD_3CH_2CD_3$	7 ± 1	0.04	12.9	
C_3D_8	6 ± 1	0.03	17.8	40 (+64/−24)

[a] Total cross section for methane and dihydrogen elimination measured at 0.05 eV. Propane adduct not included. [b] σ_{LGS} is the Langevin–Gioumousis–Stevenson collision cross section, ref 13. [c] These represent lower limits to the lifetime determined as described in ref 4. [d] Lifetime averaged over $0 < E < kT$, calculated using statistical phase space theory assuming a $Ni(propane)^+$ binding energy of 28 ± 2 kcal/mol.

Table 2. Fe^+ Reacting with Isotopically Substituted Propanes

system	total cross section (Å²)[a]	$(\sigma_{tot}/\sigma_{LGS})^b$	adduct lifetime (μs) exp[c]	adduct lifetime (μs) theory[d]
C_3H_8	14 ± 1	0.08	0.45	0.1 (+0.1/−0.05)
CH_3CHDCH_3	13 ± 1	0.07	0.64	
$CH_3CD_2CH_3$	13 ± 1	0.07	0.54	
$CH_3CH_2CD_3$	9 ± 1	0.05	1.1	
$CD_3CH_2CD_3$	4 ± 1	0.02	2.2	
C_3D_8	3 ± 1	0.02	4.2	0.7 (+1.3/−0.5)

[a] See Table 1. [b] See Table 1. [c] See Table 1. [d] Lifetime averaged over $0 < E < kT$, calculated using statistical phase space theory assuming a $Fe(propane)^+$ binding energy of 20 ± 2 kcal/mol (see ref 27).

Branching ratios at the lowest energy, 0.05 eV, between methane and hydrogen elimination are listed in Tables 3 and 4. For all systems, demethanation is favored over dehydrogenation. Deuterating the end carbons, $CH_3CH_2CD_3$ and $CD_3CH_2CD_3$, enhances dehydrogenation over demethanation relative to that observed for Ni^+ and Fe^+ reacting with C_3H_8. The effect of deuterating the central carbon, CH_3CHDCH_3 and $CH_3CD_2CH_3$, is less clear. The hydrogen/methane branching ratio for these systems and C_3H_8 are the same within the error limits of the measurement.

The isotopically labeled products for the dehydrogenation and demethanation channels are also shown in Tables 3 and 4. H_2 loss is favored over HD loss for CH_3CHDCH_3, whereas HD loss is the primary product observed for $CH_3CD_2CH_3$. For $CH_3CH_2CD_3$, H_2 elimination again dominates over HD, whereas HD accounts for nearly all of the hydrogen loss channel for $CD_3CH_2CD_3$. Demethanation for CH_3CHDCH_3 and $CH_3CD_2CH_3$ is primarily CH_4 loss, whereas about a 2:1 ratio of CD_3H and CH_3D is eliminated from Ni^+ and Fe^+ reacting with $CH_3CH_2CD_3$. For $CD_3CH_2CD_3$, CD_4 loss accounts for all of the methane loss channel.

Product distributions for metastable decomposition reactions of nascent Ni^+ and Fe^+ complexes with propane, propane-*2,2*-d_2, propane-*1,1,1,3,3,3*-d_6, and propane-d_8 are summarized in Table 5. The $M(propane)^+$ adduct is shown to increase with the extent of deuteration, consistent with the observed increase in lifetime with the extent of deuteration (see Tables 1 and 2).

(27) The relatively large uncertainty in the calculated lifetimes is due to the uncertainty in the $M(propane)^+$ binding energies, which are assumed to be 28 ± 2 kcal/mol for $Ni(C_3H_8)^+$ and 20 ± 2 kcal/mol for $Fe(C_3H_8)^+$. The $Fe(C_3H_8)^+$ binding energy was measured[51] and calculated[39] to be 20 kcal/mol with respect to the ground-state $Fe^+(^6D)$ asymptote and 26 kcal/mol with respect to the $Fe^+(^4F)$ asymptote. The $Fe(C_3H_8)^+$ lifetime averaged over $0 < E < kT$ calculated using phase space theory is too short to observe metastable decomposition assuming a binding energy of 20 kcal/mol and is within the experimental time window for metastable decomposition assuming a binding energy of 26 kcal/mol. In these calculations, the surface crossing from the $Fe^+(^4F)C_3H_8$ to the $Fe^+(^6D)C_3H_8$ is not included and may increase the actual lifetime of the complex.

Table 3. Branching Ratios for Reactions of Ni^+ with Isotopically Substituted Propanes[a]

neutral product	C_3H_8	CH_3CHDCH_3	$CH_3CD_2CH_3$	$CH_3CH_2CD_3$	$CD_3CH_2CD_3$	C_3D_8
H_2	20(2)	10(1)	3(1)[b]	14(2)	4(1)[b]	
HD		6(1)	15(2)	11(2)	21(2)	
D_2					6(1)[b]	27(2)
total	20(2)	16(2)	18(2)	25(3)	31(3)	27(2)
CH_4	80(2)	77(2)	76(2)			
CH_3D		7(1)[b]	6(1)[b]	26(3)		
CD_2H_2						
CD_3H				49(2)	3(1)[b]	
CD_4					66(2)	73(2)
total	80(2)	84(2)	82(3)	75(3)	69(2)	73(2)

[a] Measurements taken at 0.05 eV. The numbers in parentheses indicate the uncertainties. [b] These products could not be corrected unambiguously for the possibility of mass overlap from adjacent intense products and therefore could be substantially smaller or zero.

Table 4. Branching Ratios for Reactions of Fe^+ with Isotopically Substituted Propanes[a]

neutral product	C_3H_8	CH_3CHDCH_3	$CH_3CD_2CH_3$	$CH_3CH_2CD_3$	$CD_3CH_2CD_3$	C_3D_8
H_2	26(2)	17(2)	2(1)[b]	24(2)		
HD		5(1)	26(2)	9(1)	28(2)	
D_2					6(1)[b]	42(2)
total	26(2)	22(3)	28(3)	33(3)	34(3)	42(2)
CH_4	74(2)	78(2)	68(2)			
CH_3D			4(1)[b]	23(2)		
CD_2H_2						
CD_3H				44(2)		
CD_4					66(2)	58(2)
total	74(2)	78(2)	72(3)	67(4)	66(2)	58(2)

[a] See Table 3. [b] See Table 3.

Table 5. Metastable Product Distributions[a] of Nascent Fe^+ and Ni^+ Complexes with Isotopically Substituted Propanes

neutral product	metastable ion	
	$Fe(C_3H_8)^+$	$Ni(C_3H_8)^+$
H_2	31	16
CH_4	24	28
C_3H_8	45	56
	$Fe(CH_3CD_2CH_3)^+$	$Ni(CH_3CD_2CH_3)^+$
H_2	0	0
HD	6	7
CH_4	19	32
$C_3H_6D_2$	75	61(4)
	$Fe(CD_3CH_2CD_3)^+$	$Ni(CD_3CH_2CD_3)^+$
H_2	0	0
HD	22	9
D_2		1
CD_4	12	19
$C_2H_2D_6$	66	71
	$Fe(C_3D_8)^+$	$Ni(C_3D_8)^+$
D_2	~1	7
CD_4	~1	29
C_3D_8	98	64

[a] The uncertainty in the product distribution, based on the reproducibility, is ±4.

Statistical phase space theory[14,15] is used to model both the reaction efficiency and the experimental kinetic energy release distributions. The calculations have been described previously, and a summary is given in the Appendix. One purpose of the calculations is to determine whether a statistical model, which assumes a potential energy surface without a barrier to the reverse association in the exit channel, is adequate to describe the experimental kinetic energy release distribution. A second purpose of the calculations is to model the potential energy surface and determine, if possible, the nature and energies of important tight transition states.[12,28] The parameters used in the phase space calculations are summarized in Table 7.

Table 6. Reaction Enthalpies and Average Kinetic Energy Releases from Experiment and Phase Space Theory

reaction	$-\Delta H$ (eV)[a]	$\bar{E}_t$ (eV) expt	$\bar{E}_t$ (eV) theory[b]
$Ni^+ + C_3H_8 \rightarrow Ni(C_3H_6)^+ + H_2$	0.65	0.38	0.093
$Ni^+ + C_3H_8 \rightarrow Ni(C_2H_4)^+ + CH_4$	1.11	0.10	0.107[c] (0.15)[d]
$Ni^+ + C_3D_8 \rightarrow Ni(C_2D_4)^+ + CD_4$	1.11	0.11	0.098[e]
$Fe^+ + C_3H_8 \rightarrow Fe(C_3H_6)^+ + H_2$	0.39	0.30	0.076
$Fe^+ + C_3H_8 \rightarrow Fe(C_2H_4)^+ + CH_4$	0.74	0.08	0.085[c] (0.13)[d]
$Fe^+ + C_3D_8 \rightarrow Fe(C_2D_4)^+ + CD_4$	0.74		0.079[e]

[a] Heat of reaction at 0 K, deuterium effects are assumed negligible. [b] Statistical phase space theory using the methods outlined in ref 12. [c] Statistical phase space theory with a barrier for initial C–H bond insertion located 0.10 and 0.075 eV below the Ni^+/C_3H_8 and the Fe^+/C_3H_8 asymptotic energies respectively (see Figure 1). [d] Statistical phase space theory without a C–H insertion barrier included. [e] Statistical phase space theory with a barrier for initial C–D bond insertion located 0.053 and 0.028 eV below the Ni^+/C_3D_8 and the Fe^+/C_3D_8 asymptotic energies, respectively.

The calculated and experimental average kinetic energy releases, $\bar{E}_t$, are presented in Table 6. For H_2 elimination from the $Ni(C_3H_8)^+$ and $Fe(C_3H_8)^+$ adducts, the experimental $\bar{E}_t$ is much larger than the calculated value, whereas for CH_4 elimination, the experimental and theoretical values for $\bar{E}_t$ are essentially the same. The KERDs obtained for H_2 elimination are bimodal, as shown in Figures 3a and 3b. The high kinetic energy release component is significantly more intense for the iron system than for the nickel system. Also shown are the KERDs obtained from statistical phase space theory modeling. The low-energy component for H_2 elimination from $Fe(C_3H_8)^+$ is very nearly statistical, whereas both the low- and high-energy components for H_2 loss from $Ni(C_3H_8)^+$ appear to be significantly broader than statistical.

The KERDs for CH_4 loss from Ni(propane)$^+$ and Fe(propane)$^+$ are shown in Figures 4a and 4b. The observed distributions are narrower than those predicted by unrestricted statistical phase space theory. The "unrestricted" phase space theory curves

(28) Graul, S. T.; Bowers, M. T. *J. Am. Chem. Soc.* **1991**, *113*, 9697.

Table 7. Input Parameters Used in Calculations[a] for M = Ni and Fe

	$MC_2H_4^+$	$M^+\cdots C_3H_8$[b]	$MC_3H_6^+$	$MC_2D_4^+$	$M\cdots C_3D_8$[b]
$\Delta H_f°_0$[c]	249.4[d]	256.7[d,e]	244[d]	249.2[d]	256.7[d,e]
	(260.0)[f]	(259.3)[e,f]	(252)[f]	(260.0)[f]	(260.4)[e,f]
B[g]	0.32	0.19[h]	0.16	0.26	0.15[h]
σ[i]	2	1	1	2	1
ν_i[j]	3106	2973[k]	3090	2345	2224(2)[k]
	3103	2968(2)	3013	2304	2221
	3026	2967	2991	2259(3)	2149
	3019(3)	2962	2954	2251	2122
	2989	2887(2)	2932	2200	2081(2)
	2917	1476	2871	2109	1203
	1623	1472	1650	1515	1086(3)
	1534(2)	1464	1470	1092(2)	1064(4)
	1444	1462	1443	1078	959
	1342	1451	1420	1009	949
	1306(3)	1392	1378	996(3)	945
	1236	1378	1299	981	862
	1023	1338	1171	780	712
	949	1278	1045	728	688
	943	1192	991	720	659
	826	1158	963	586	544
	300	1054	920	300	332
	250	940	912	250	250
	200	922	578	200	200
		869	428		172
		748	300		150
		369	250		143
		268	200		
		250	174		
		216			
		200			
		150			

[a] Input parameters for H_2, CH_4, CD_4, C_3H_8, and C_3D_8 have been published (ref 12). [b] C–H(D) bond activation transition-state complex. [c] Heat of formation at 0 K in kcal/mol (refs 34, 59, 61, 62). [d] Heat of formation for $NiC_xH_y^+$, all other parameters are the same for Fe and Ni. [e] Rough estimate. Calculated assuming $\Delta E^‡(Ni^+\cdots C_3H_8) = 0.10$ eV, $\Delta E^‡(Ni^+\cdots C_3D_8) = 0.053$ eV, $\Delta E^‡(Fe^+\cdots C_3H_8) = 0.075$ eV, $\Delta E^‡(Fe^+\cdots C_3D_8) = 0.028$ eV. [f] Heat of formation for $FeC_xH_y^+$, all other parameters for Fe are the same as for Ni. [g] Rotational constant in cm^{-1}. [h] Rotational constant assuming the metal ion coordiantes with primary hydrogens in the plane of propane. [i] Symmetry number. [j] Vibrational frequencies in cm^{-1}. [k] One C–H(D) frequency becomes the reaction coordinate, breaking the C–H(D) bond. Hence, the number of frequencies, ν_i, is equal to $3N-7$, where N is the number of atoms in the molecule.

assume that the entrance and exit channels contain only orbiting transition states and that there are no tight transition states in between that affect the dynamics. The "restricted" phase space theory calculations shown in the figures include a tight transition state for insertion into a C–H bond located 0.075 and 0.10 eV below the asymptotic energies of the reactants for iron and nickel, respectively, and good agreement between experiment and theory is obtained. The theoretical KERD is sensitive to the energy of the tight transition state, and reasonable agreement with experiment is obtained only for $\Delta E^‡ < 0.085$ eV and $\Delta E^‡ < 0.11$ eV for iron and nickel, respectively.

The theoretical KERD for H_2 elimination (Figure 3) was calculated with and without implementation of a barrier for C–H insertion. The significant angular momentum restriction observed for methane elimination (Figure 4), due to the C–H insertion barrier, is not observed for H_2 elimination. This occurs because loss of H_2 from the $M(C_3H_8)^+$ complex is already restricted to low angular momenta, due to the low mass and polarizability of H_2, independent of restrictions imposed by the C–H insertion transition state.

Discussion

A. Absolute Cross Sections for Fe^+ and Ni^+ Reacting with Propane and Labeled Propanes. For both Fe^+ and Ni^+ reacting with propane, dehydrogenation and demethanation channels are strongly exothermic (Table 6), and the shapes of the energy-dependent cross sections (Figure 2) indicate no barriers exceeding the asymptotic energy of the reactants. Consequently, the observed inefficiency of these reactions indicates that rate-limiting transition states exist along the reaction coordinate with energies near the asymptotic energy for both iron and nickel. The large decrease in the cross section with the extent of deuteration for both dehydrogenation and demethanation implies the rate-limiting transition state is associated with a C–H bond for both product channels.

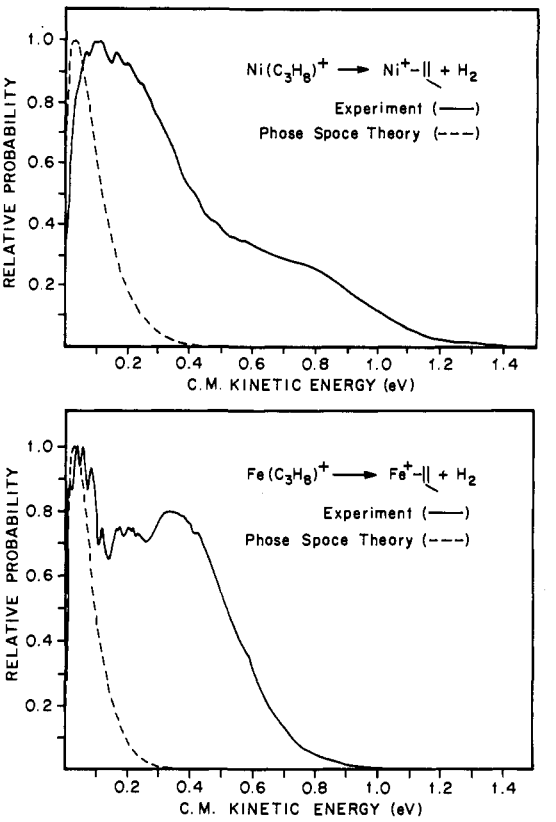

Figure 3. Kinetic energy release distribution for metastable loss of H_2 from nascent (a, top) $Ni(C_3H_8)^+$ and (b, bottom) $Fe(C_3H_8)^+$ collision complexes. The solid line labeled "experiment" results from analysis of the laboratory peak shape using standard techniques (ref 23). The dashed line results from phase space theory calculations, including a barrier for initial C–H insertion.

Two mechanisms have been proposed for dehydrogenation and demethanation channels for metal ions, M^+, reacting with propane as shown in Scheme 1.[5,12,29] For dehydrogenation, initial primary C–H bond activation followed by β-H transfer is proposed to form the dihydride propene complex **1**, which reductively eliminates H_2, whereas initial secondary C–H bond activation is proposed to involve a concerted H_2 elimination process via the multicenter transition state indicated in Scheme 1. For demethanation, either initial C–C bond activation followed by β-H transfer or initial primary C–H bond activation followed by β-CH_3 transfer forms the metal methyl hydride ethene complex **2**, which reductively eliminates CH_4.

There are two compelling pieces of experimental evidence for rate-limiting transition states along the reaction coordinate in these systems: (1) the reactions are inefficient when compared to the collision theory prediction and (2) there is a very strong isotope effect when D is substituted for H in either the primary or secondary positions in propane. The first of these effects could be due to any transition state, but the second requires a transition

(29) See, for example: (a) Armentrout, P. B.; Beauchamp, J. L. *J. Am. Chem. Soc.* **1981**, *103*, 784. (b) Elkind, J. L.; Armentrout, P. B. *J. Phys. Chem.* **1985**, *89*, 5626. (c) Sunderlin, L.; Aristov, N.; Armentrout, P. B. *J. Am. Chem. Soc.* **1987**, *109*, 78. (d) Georgiadis, R.; Fisher, E. R.; Armentrout, P. B. *J. Am. Chem. Soc.* **1989**, *111*, 4251.

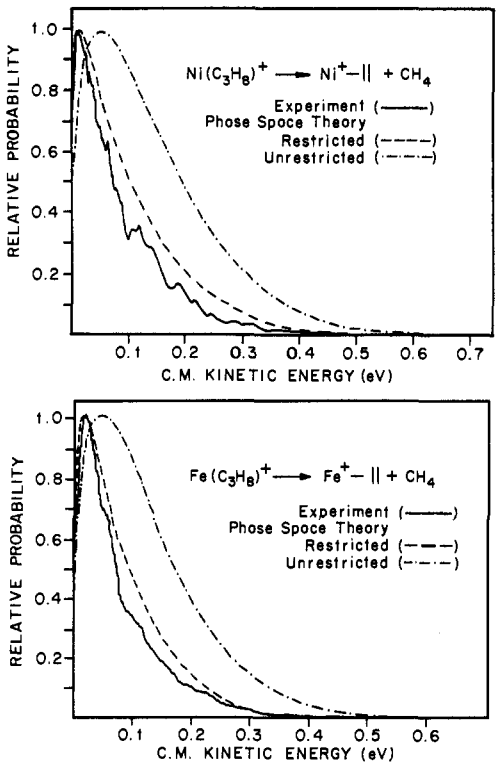

Figure 4. Kinetic energy release distribution for metastable loss of CH_4 from nascent (a, top) $Ni(C_3H_8)^+$ and (b, bottom) $Fe(C_3H_8)^+$ collision complexes. The "unrestricted" phase space theory curve assumes the entrance channel contains only an orbiting transition state, the exit channel has only an orbiting transition state (no reverse activation barrier), and there are no tight transition states in between that affect the dynamics. The "restricted" phase space theory calculation includes a tight transition state for insertion into a C–H bond located 0.10 and 0.075 eV below the asymptotic energy of the reactants for Ni^+ and Fe^+, respectively (see text).

Scheme 1

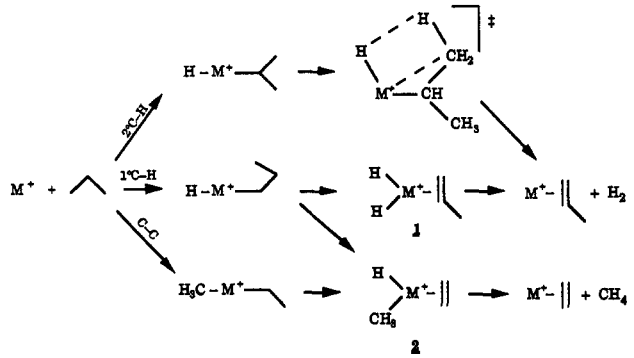

state associated with breaking or making a C–H (C–D) bond. Arguments that this transition state is associated with the initial C–H bond insertion following the $M(C_3H_8)^+$ electrostatic complex were convincingly made for the Co^+/C_3H_8 system.[12] It was pointed out that Co^+ did not react with ethane at thermal energy, even though H_2 elimination is exoergic. The reason given was that initial insertion into the C–H bond did not occur, a conclusion consistent with the fact that CID of $Co(C_2H_6)^+$ adducts yields essentially 100% $Co^+ + C_2H_6$ products.[30] Insertion is believed to occur for propane because $Co(C_3H_8)^+$ electrostatic stabilization is sufficient to bring the insertion barrier below the $Co^+ + C_3H_8$ asymptotic energy. Similar reasoning applies to the Fe^+ and Ni^+ reactions discussed in this paper. As observed for $Co(C_2H_6)^+$, threshold collisional activation of $Fe(C_2H_6)^+$ adducts yield essentially 100% $Fe^+ + C_2H_6$ products,[31] again indicating that the interaction of Fe^+ with ethane is not strong enough to overcome intrinsic barriers that may be associated with insertion into a C–H or C–C bond. As a result, H_2 elimination is not observed for Fe^+ reacting with C_2H_6 even though the reaction is exoergic.[32] Again, the electrostatic stabilization of $Fe(C_3H_8)^+$ is sufficient to bring the insertion barrier below the Fe^+ + propane reactant energy. Even though this suggests that initial C–H bond activation is the rate-limiting transition state, β-H transfer and reductive elimination of H_2 or CH_4 (involving H–H or C–H coupling) are also possible rate-limiting transition states. The evidence for or against each of these transition states as rate limiting will be considered in the following sections.

B. Metastable Dissociation of Nascent Fe(Propane)$^+$ and Ni(Propane)$^+$ Complexes. 1. 1,2-Hydrogen Elimination. The KERDs for H_2 elimination from $Fe(C_3H_8)^+$ and $Ni(C_3H_8)^+$ are clearly nonstatistical and have pronounced bimodality. The broader than statistical kinetic energy release indicates that a tight transition state near the exit channel dominates the dynamics for product formation. The bimodality signifies two distinct decomposition processes. As observed for Co^+ reacting with C_3H_8, both primary and secondary C–H bond activation followed by β-H transfers are possible mechanisms for H_2 elimination (Scheme 1). The question is whether these two mechanisms are responsible for the bimodal KERD for Ni^+ and Fe^+ reacting with C_3H_8.

In order to gain some insight into the details of the mechanism, KERDs using propane-*2,2-*d_2, propane-*1,1,1-*d_3, propane-*1,1,1,3,3,3-*d_6, and propane-d_8 were obtained. The KERDs for HD loss from Fe^+ reacting with propane-*2,2-*d_2 and propane-*1,1,1,3,3,3-*d_6 are shown in Figures 5a and 5b along with those for H_2 loss from $Fe(C_3H_8)^+$. For propane-*2,2-*d_2, the high-energy component in the KERD is substantially reduced for HD loss in comparison to H_2 loss from $Fe(C_3H_8)^+$. For propane-*1,1,1,3,3,3-*d_6, however, the low-energy component is significantly reduced for HD loss in comparison to HD loss from propane-*2,2-*d_2. Similar isotope effects on the KERDs for HD loss in comparison to H_2 loss are observed for Ni(propane)$^+$ complexes (shown in Figures 6a and 6b).

The difference in energy between high- and low-energy components in the KERDs for dehydrogenation is quite large, approximately 0.4 eV. The high-energy component is much broader than the statistical distribution, suggesting a large barrier in the exit channel. For HD loss from $Fe(CH_3CD_2CH_3)^+$, the substantial reduction in the high-energy component effectively deconvolutes the two decomposition processes in the KERD such that the low-energy component now appears statistical (see Figure 5a). For HD loss from $Ni(CH_3CD_2CH_3)^+$, the reduction in the high-energy component is not large enough to deconvolute the two decomposition processes, although the distribution is narrower relative to H_2 loss from $Ni(C_3H_8)^+$ (Figure 6a).

The substantial reduction of the low- and high-energy components when D replaces H in the primary and secondary positions in propane (Figures 5 and 6) is consistent with the initial primary and secondary C–H(D) insertion barriers both being near the asymptotic energies of the reactants. The energy of either transition state increases (due to zero-point effects) when D replaces H, thereby strongly reducing the flux through it relative to the C–H insertion transition state with which it competes.

The possibility that the β-H transfer transition state or the H–H coupling transition states might be rate limiting needs to be considered. The low-energy component in the KERD for dihydrogen loss indicates that one of the dehydrogenation processes does not involve a high-energy transition state near the

(30) Armentrout, P. B., personal communication.

(31) Schultz, R. H.; Armentrout, P. B. *J. Phys. Chem.* **1992**, *96*, 1662.

(32) Byrd, G. D.; Burnier, R. C.; Freiser, B. S. *J. Am. Chem. Soc.* **1982**, *104*, 3565, Halle, L. F.; Armentrout, P. B.; Beauchamp, J. L. *Organometallics* **1982**, *1*, 963 and Tonkyn et al. (ref 6) do not observe H_2 elimination for Fe^+ reacting with C_2H_6 at thermal energies. Schultz et al. (ref 5), however, do observe H_2 elimination but find the reaction to be extremely inefficient (occurring less than once in every 1000 collisions), and it is possible that this is due to electronically excited states.

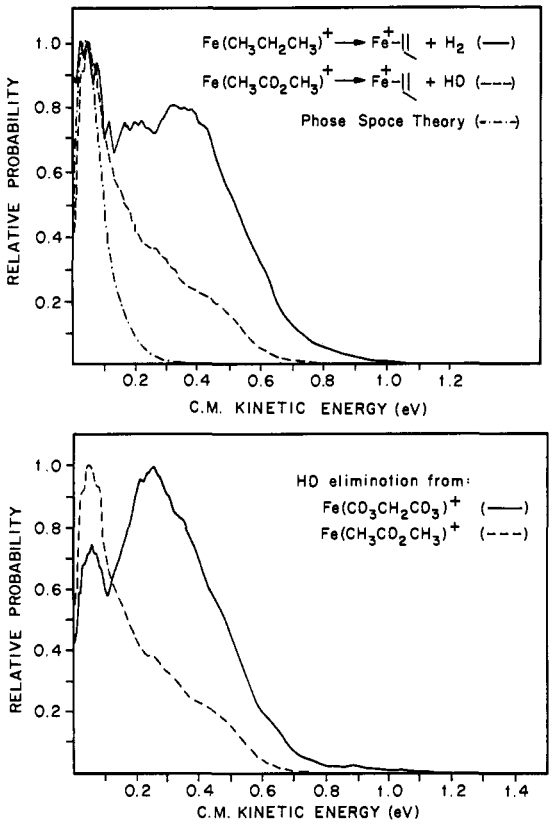

Figure 5. (a, top) Product kinetic energy release distributions for metastable loss of H_2 from nascent $Fe(C_3H_8)^+$ (solid line) and HD from nascent $Fe(CH_3CD_2CH_3)^+$ (dashed line). The phase space theory prediction is given by the dash-dot line. (b, bottom) Kinetic energy release distributions for metastable loss of HD loss from $Fe(CD_3CH_2CD_3)^+$ (solid line) and HD loss from $Fe(CH_3CD_2CH_3)^+$ (dashed line).

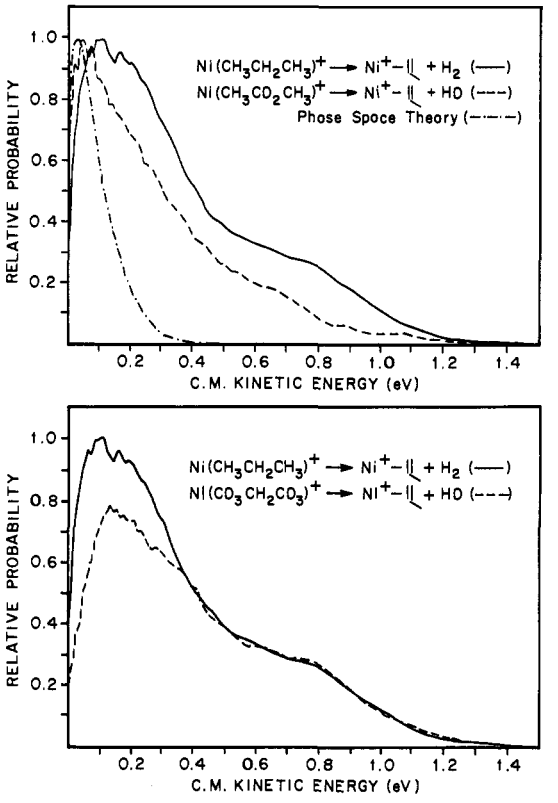

Figure 6. (a, top) Product kinetic energy release distributions for metastable loss of H_2 from nascent $Ni(C_3H_8)^+$ (solid line) and HD from nascent $Ni(CH_3CD_2CH_3)^+$ (dashed line). The phase space theory prediction is given by the dash-dot line. (b, bottom) Kinetic energy release distributions for metastable loss of H_2 from $Ni(C_3H_8)^+$ (solid line) and HD loss from $Ni(CD_3CH_2CD_3)^+$ (dashed line).

exit channel. H–H coupling from a metal propene dihydride intermediate (structure **1**, Scheme 1) is most likely responsible for the statistical component in the KERD. Theoretically, reductive elimination of H_2 is predicted to have a small activation energy[33] and consequently may lead to a statistical decomposition process.

The strong decrease in the high- and low-energy components in the KERDs for HD loss from $CH_3CD_2CH_3$ and $CD_3CH_2CD_3$, especially for the Fe^+ system (Figure 5b), indicates that no significant isotopic scrambling is taking place. In addition, no significant isotopic scrambling is observed in the branching ratios (Tables 3 and 4). This argues against the final H–H(D) reductive coupling transition state being rate limiting. The β-H shift transition state is also unlikely to be rate limiting based on two observations. First, we conclude in the next section that initial primary C-H bond activation is rate limiting for the CH_4 loss reaction rather than the β-CH_3 shift transition state. Second, β-H transfer from the H–M^+–$CH_2CH_2CH_3$ intermediate should be more facile than β-CH_3 transfer (due to the spherically symmetric s orbital on H versus the directional sp^3 hybrid orbital on CH_3)[33] and hence cannot be rate limiting. We therefore conclude that the primary C–H insertion transition state is rate limiting for H_2 elimination. Because secondary C–H bonds of propane are only 1.7 kcal/mol weaker than primary C–H bonds, initial secondary C–H bond activation is expected to be rate limiting as well. This conclusion is consistent with the relative change in the KERD for HD loss from $CH_3CD_2CH_3$ and $CD_3CH_2CD_3$, as shown in Figures 5 and 6.

These results are very similar to those of Co^+ reacting with propane and deuterated propanes,[12] and consequently the mechanisms of the three systems are likely to be similar. A schematic reaction coordinate diagram for H_2 elimination that summarizes our conclusions is shown in Figure 7.

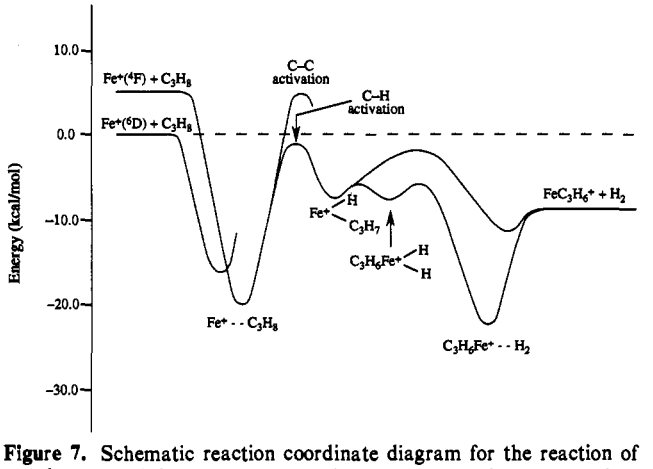

Figure 7. Schematic reaction coordinate diagram for the reaction of $Fe^+(^6D)$ and $Fe^+(^4F)$ with propane via initial primary and initial secondary C–H bond activation to eliminate H_2.

2. Methane Elimination: The Rate-Limiting Transition State. For demethanation, either initial C–C bond activation followed by β-H transfer or initial primary C–H bond activation followed by β-CH_3 transfer leads to reductive elimination of CH_4 (Scheme 1). The possibility that the transition state associated with the CH_4 reductive elimination step might be rate limiting needs to be considered, because this step involves making a C–H bond. Because the isotope effect is so large (Tables 1 and 2) and the overall reaction is inefficient, this transition state would need to be near the asymptotic $M^+ + C_3H_8$ energy. This seems unlikely for Co^+ and Ni^+ because the reactions are about 24 and 26 kcal/

(33) Low, J. J.; Goddard, W. A. *J. Am. Chem. Soc.* **1984**, *106*, 8321.

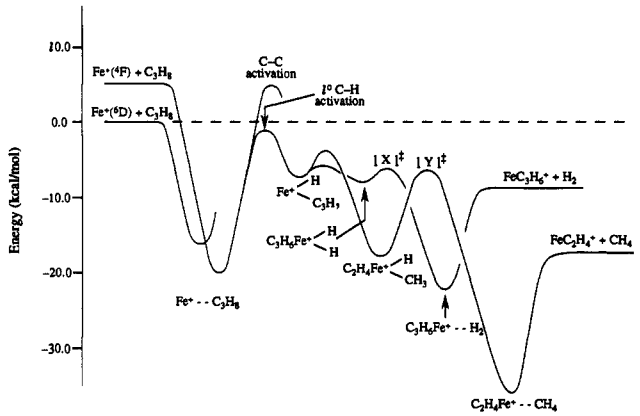

Figure 8. Schematic reaction coordinate diagram for the reaction of $Fe^+(^6D)$ and $Fe^+(^4F)$ with propane via initial primary C–H bond activation to eliminate CH_4 and H_2.

mol exoergic.[12,34] When the $C_2H_4M^+$–CH_4 stabilization energy of 24 ± 4 kcal/mol[35] is added, a transition-state energy of nearly 50 kcal/mol (relative to $C_2H_4M^+$–CH_4) would be required for insertion of $C_2H_4M^+$ into the C–H bond of CH_4 if the transition state is to be near the $M^+ + C_3H_8$ asymptotic energy. When one considers the fact M^+ ions can insert into a C–H bond in propane with less than a 30 kcal/mol barrier relative to the $M(C_3H_8)^+$ energy,[36,37] it appears likely that the CH_4 reductive elimination transition state is well below the $M^+ + C_3H_8$ asymptotic energy. Hence, reductive elimination transition states are not believed to be rate determining for M = Co or M = Ni.

For Fe^+ reacting with propane, the CH_4 elimination channel is only 17 kcal/mol exoergic.[34] Assuming that the stabilization of energy for $C_2H_4Fe^+$–CH_4 is similar to that for CH_4Fe^+–CH_4, which is 23.3 ± 1.0 kcal/mol,[38] a barrier height of about 40 kcal/mol relative to the bottom of the $C_2H_4Fe^+$–CH_4 well is required if reductive elimination is to become rate limiting (see Figure 8). This still seems too large, however, when one considers that Fe^+ does insert into the C–H bonds of C_3H_8 and that the $Fe(C_3H_8)^+$ stabilization energy for ground-state $Fe^+(^6D, 4s3d^6)$ is on the order of 20 kcal/mol[39] (even when the difference in C–H bond energies between methane and propane is considered).[40]

The CH_4/H_2 branching ratios (Tables 3 and 4) indicate that CH_4 elimination is favored over H_2 elimination by a factor of 4.0 and 2.8, respectively, for Ni^+ and Fe^+ reacting with C_3H_8. As discussed in the last section, the lack of isotopic scrambling suggests that the final H–H reductive elimination transition state is not rate limiting for H_2 loss. If the final reductive elimination transition state for CH_4 loss were rate limiting, H_2 loss would be favored over CH_4 loss, a conclusion inconsistent with the branching ratio observed. A schematic reaction coordinate diagram for initial primary C–H bond activation leading to H_2 and CH_4 elimination is shown in Figure 8. We believe that the relative energies of the reductive elimination transition states, denoted as $[X]^‡$ and $[Y]^‡$ in Figure 8, primarily determine the CH_4/H_2 branching ratio. Thus, it seems very likely that the C–H reductive coupling transition state for CH_4 loss is lower in energy than the H–H coupling transition state and that the initial C–H insertion transition state must be rate limiting.

Finally, we must consider initial C–C bond activation as a possible mechanism for methane loss. If initial C–C bond activation contributes significantly to the mechanism for methane loss, then β-hydrogen transfer must be rate limiting to account for the H,D isotope effect. However, consideration of the thermochemistry of the putative $CH_3MC_2H_5^+$ and $HMC_3H_7^+$ intermediates indicates that β-hydrogen transfer is most probably not the rate-limiting transition state for methane elimination. Initial C–C bond activation to form the $CH_3MC_2H_5^+$ intermediate involves breaking a C–C bond of propane (86 kcal/mol at 0 K)[40] and forming M^+–CH_3 and CH_3M^+–C_2H_5 bonds. Initial primary C–H bond activation to form the $HMC_3H_7^+$ intermediate involves breaking a primary C–H bond of propane (98 kcal/mol at 0 K)[40] and forming M^+–H and HM^+–C_3H_7 bonds. The intrinsic M^+–CH_3 and M^+–H bond strengths are 58 and 55 kcal/mol, respectively.[41-48] Taking into account the promotion energy,[41,49,50] the energies of the $HMC_3H_7^+$ intermediates are estimated to lie near the energies of Fe^+, Co^+, and Ni^+ plus propane reactants. The intrinsic bond energy for M^+–C_2H_5 is the same as that for M^+–CH_3, 58 kcal/mol, and is expected to be similar for M^+–C_3H_7. Thus, the $CH_3MC_2H_5^+$ intermediate is about 15 kcal/mol more stable than the $HMC_3H_7^+$ species. Consequently, the β-H transfer transition state from $CH_3MC_2H_5^+$ is up to 15 kcal/mol lower in energy than the comparable β-H transfer transition state from $HMC_3H_7^+$ and is unlikely to show an appreciable H/D isotope effect for methane loss. Based on the conclusion that C–H insertion is important, it follows that initial C–C insertion is probably not an important process at thermal energies for Fe^+, Co^+, and Ni^+ reacting with C_3H_8. Consequently, initial primary C–H bond activation is most likely the rate-limiting transition state for CH_4 and H_2 elimination, and initial C–C bond activation does not contribute significantly at low energies.

(34) The metal ion–olefin bond energies are discussed in the Appendix and in refs 59, 61, and 62.

(35) The binding energy of $C_2H_6Co^+$–CH_4 has been measured to be 24 ± 4 kcal/mol, and it is expected that $C_2H_4Co^+$–CH_4 would be bound by a similar amount. Kemper, P. R.; Bushnell, J.; van Koppen, P. A. M.; Bowers, M. T. *J. Phys. Chem.* **1993**, *97*, 1810.

(36) Perry, J. K.; Ohanessian, G.; Goddard, W. A. *J. Phys. Chem.* **1993**, *97*, 5238.

(37) Haynes, C.; Armentrout, P. B., work in progress.

(38) Schultz, R. H.; Armentrout, P. B. *J. Phys. Chem.* **1993**, *97*, 596.

(39) Perry, J. K.; Goddard, W. A., personal communication.

(40) Lias, S. G.; Bartmess, J. E.; Liebman, J. F.; Holmes, J. L.; Levin, R. D.; Mallard, W. G. *J. Phys. Chem. Ref. Data* **1988**, *17* (Suppl. 1).

(41) The intrinsic bond energy is obtained by plotting the M^+–L bond dissociation energies (BDEs), for M = Sc through Zn, as a function of the promotion energy, E_p, and by applying a linear regression analysis of these data.[42-46] To determine the bond energy of the CH_3–M^+–C_2H_5 and H–M^+–C_3H_7 intermediates for a specific metal, the sum of the intrinsic bond energies must be corrected for the promotion energy. For two covalent bonds, this promotion energy is defined as the energy required to take the metal ion in its ground state to an s^1d^{n-1} electron configuration where the s and one d electron are spin-decoupled from the remaining metal d electrons.[42,45,46] For Fe^+, Co^+, and Ni^+, the promotion energies calculated by Carter and Goddard[49] are essentially the same, 41.4, 39.2, and 41.6 kcal/mol, respectively. Correlations of promotion energies with a large series of experimental M^+—L, M^+=L, and M^+—L_2 BDEs for M = Sc through Zn show that only a fraction (0.5 ± 0.05) of the promotion energy is needed to account for the variations in BDEs from the intrinsic BDEs.[42,45,46] Thus, the empirical correction yields H–M^+–C_3H_7 BDEs to be 55 + 58 – 0.5(E_p) = 92, 93, and 92 kcal/mol for Fe, Co, and Ni, respectively, and CH_3–M^+–C_2H_5 to be 58 + 58 – 0.5(E_p) = 95, 96, and 95 kcal/mol for Fe, Co, and Ni, respectively. The fact that only a fraction of the promotion energy is subtracted from the intrinsic bond energies can be rationalized by considering that the calculated promotion energies[49] do not include state mixing, which can reduce these promotion energies significantly.[50] At this point, our best estimates for the BDEs of CH_3–M^+–C_2H_5 and H–M^+–C_3H_7 are obtained by using the empirical formula shown above. From these BDE estimates, C–H bond activation is determined to be slightly endoergic, by about 5 kcal/mol for Fe^+, Co^+, and Ni^+ reacting with propane. However, these reactions could well be exoergic given the uncertainty of the BDE measurements and of the promotion energy correction. Hence we do not feel that these estimates rule out C–H bond activation as the initial step of the reaction, and we feel that the weight of the remaining evidence continues to point to C–H bond activation as the rate-limiting step at thermal energies.

(42) Armentrout, P. B.; Kickel, B. L. In *Organometalic Ion Chemistry*; Freiser, B. S., Ed.; Kluwer Academic Publishers: The Netherlands, in press.

(43) Armentrout, P. B.; Halle, L. F.; Beauchamp, J. L. *J. Am. Chem. Soc.* **1981**, *103*, 6501.

(44) Mandich, M. L., Halle, L. F., Beauchamp, J. L. *J. Am. Chem. Soc.* **1984**, *106*, 4403.

(45) Elkind, J. L., Armentrout, P. B. *Inorg. Chem.* **1986**, *25*, 1078.

(46) Armentrout, P. B.; Georgiadis, R. *Polyhedron* **1988**, *7*, 1573.

(47) Bauschlicher, C. W., Jr.; Langhoff, S. R. *Int. Rev. Phys. Chem.* **1990**, *9*, 149.

(48) Bauschlicher, C. W., Jr.; Langhoff, S. R.; Partridge, H. *Modern Electronic Structure Theory*; Yarkony D. R., Ed.; World Scientific Publishing Company: London, in press.

(49) Carter, E. A.; Goddard, W. A. *J. Phys. Chem.* **1988**, *92*, 5679. Table 3 of this reference lists values for E_{lost}, equivalent to E_p in this paper.

(50) Bauschlicher, C. W., Jr.; Walch, S. P. *J. Chem. Phys.* **1983**, *78*, 4597.

The fact that we fail to observe initial C–C bond activation at low energy is consistent with threshold collisional activation data for $Fe(C_3H_8)^+$, where the C–C bond activation transition state was determined to be ~8 kcal/mol above the C–H bond activation transition state.[51] These results can be rationalized by using the results of Low and Goddard,[33] who determined relative transition-state energies for reductive H–H, C–H, and C–C coupling to eliminate H_2, CH_4, and C_2H_6 from the corresponding Pt and Pd complexes. Due to the directionality of the sp^3 hybrid orbital on carbon versus the spherically symmetric s orbital on hydrogen, the transition state for C–C reductive coupling was calculated to be 10 kcal/mol higher than that for C–H reductive coupling, which in turn was 10 kcal/mol higher than the H–H transition state. Blomberg et al.[52] extended these calculations to include both first and second row transition metals, Fe, Co, Ni, Rh, and Pd. For all these metals, the transition state for C–C bond activation in ethane was found to be 14–20 kcal/mol higher than that for C–H bond activation in methane. In the next section, we conclude that the transition state for initial C–H bond activation for Fe^+ and Ni^+ reacting with propane is only a few kcal/mol below the reactant energy. Thus, if the initial C–C bond activation transition state is 10–20 kcal/mol higher in energy than C–H bond activation, it will be located ~8–18 kcal/mol above the reactant energy. Such a high transition-state energy would explain why initial C–C bond activation would not occur at low energy.

3. Methane Elimination: The Rate-Limiting Transition-State Energy. The KERDs for methane elimination from $Ni(C_3H_8)^+$ and $Fe(C_3H_8)^+$ (Figures 4a and 4b) are narrower than those predicted by "unrestricted" statistical phase space theory. "Unrestricted" statistical phase space theory assumes that the entrance and exit channels contain only orbiting transition states and that there are no tight transition states along the reaction coordinate that affect the dynamics. In this case, the angular momentum constraints are determined by the orbiting transition state in the entrance channel. However, as discussed earlier, the inefficiency of these reactions as well as the H,D isotope effect indicates that a rate-limiting transition state, most probably associated with initial primary C–H bond activation, does exist along the reaction coordinate for demethanation. This tight transition state imposes more restrictive angular momentum constraints, decreasing the average kinetic energy released for methane elimination.[12] The "restricted" phase space theory calculations include a tight transition state for insertion into the C–H bond. The KERD is calculated as a function of the barrier height, $\Delta E^\ddagger$, locating the C–H insertion transition state relative to the asymptotic energy of the reactants (see Figure 1). The upper limits on $\Delta E^\ddagger$ determined by modeling the KERD for methane elimination are 0.08 and 0.11 eV for iron and nickel, respectively.

A lower limit on $\Delta E^\ddagger$ is obtained by modeling the H,D isotope effect on the absolute cross sections. The maximum difference in the transition-state energies for the protonated and deuterated systems is simply the difference in zero point energies for the C–H and C–D bonds:

$$\Delta E_H^\ddagger - \Delta E_D^\ddagger = {}^1/_2 h(\nu_{CH} - \nu_{CD}) = 0.047 \text{ eV} \qquad (1)$$

When this energy shift is incorporated into the phase space calculations for Fe^+ and Ni^+ reacting with propane (along with appropriately changing all the frequencies and the rotational constant for deuteration), the theoretical prediction of the relative reaction efficiency, $\gamma(C_3H_8)/\gamma(C_3D_8)$, where $\gamma = k_{products}/k_{collision}$, is indicated in eq 2:

$$Fe^+, \ \frac{\gamma(C_3H_8)}{\gamma(C_3D_8)} = 4.5 \pm 0.4 \quad Ni^+, \ \frac{\gamma(C_3H_8)}{\gamma(C_3D_8)} = 3.0 \pm 0.4 \qquad (2)$$

These results are in good agreement with experiment (4.4 ± 0.6 and 3.8 ± 0.6 for Fe^+ and Ni^+, respectively) and serve as further evidence for the proposed model. The cross section is very sensitive to the frequencies used for the C–H bond activation transition state. The range in frequencies, however, is relatively small because of the upper limit on $\Delta E^\ddagger$ determined by modeling the KERD. In addition, the range in frequencies used is consistent with recent ab initio calculations by Perry et al.[36] on $Co(C_3H_8)^+$ complexes. The acceptable range of values in $\Delta E^\ddagger$ is 0.075 ± 0.01 and 0.10 ± 0.01 for Fe^+ and Ni^+, respectively.

In this analysis, we have assumed that the effect of excited spin–orbit states is negligible on the KERDs and that $\Delta E^\ddagger$ is referenced to the ground spin–orbit state for Fe^+, Co^+, and Ni^+ reacting with propane. We can consider alternate assumptions by examining the $Ni^+ + C_3H_8$ reaction. One possibility is that the ground and excited spin–orbit states react on parallel surfaces, in which case there would be no way to distinguish these processes in the KERDs and there would be two transition states, each lying $\Delta E^\ddagger$ below its associated $Ni^+ + C_3H_8$ asymptote. It seems more likely, however, that the large size of the propane ligand and the long lifetime of the $NiC_3H_8^+$ adduct will enable coupling of the spin–orbit energy into the complex. (This seems especially likely given the observation that He and Ne have been found to quench spin–orbit excitation.)[53] There is a 0.19 eV difference in energy in the two spin–orbit states of $Ni^+(^2D)$, enough that a bimodal distribution in the KERD for CH_4 loss would be observed, assuming that both spin–orbit states of Ni^+ react with propane to eliminate CH_4 on a time scale of 6–14 μs. However, the calculated lifetime for a $NiC_3H_8^+$ complex with an additional 0.19 eV of excitation is 100 times shorter than that without this extra energy. This is sufficiently short that such excited complexes will decompose prior to the magnet, leading to the unimodal KERD observed in our experiments.

It is also possible that the ground spin–orbit state does not react at thermal energy because the energy of the C–H bond activation transition state is above the asymptotic energy of the ground spin–orbit state of $Ni^+ + C_3H_8$ reactants. $\Delta E^\ddagger$ would then be relative to the excited spin–orbit state. In this case, however, the ground spin–orbit state would be able to react at translational energies above the transition state. Given that surface ionization produces a beam containing 20% excited spin–orbit state of Ni^+ and 80% ground spin–orbit state, such an endothermic feature would be easily observed in the cross sections, but there is no evidence for anything but barrierless elimination of H_2 and CH_4.

C. Branching Ratios. Evidence has been presented that at low kinetic energy in M^+/C_3H_8 systems, CH_4 loss proceeds through a rate-determining transition state associated with initial primary C–H bond activation for both M = Fe and M = Ni. H_2 loss, however, proceeds via both initial primary and initial secondary C–H bond activation, both of which are rate-limiting transition states. The branching ratios for all the isotopic variants shown in Tables 3 and 4 support these results. The cross sections drop for both demethanation and dehydrogenation when either the central or the end carbons are deuterated. Demethanation is favored over dehydrogenation for both Fe^+ and Ni^+ reacting with propane and labeled propanes. The enhancement of dehydrogenation over demethanation by deuterating the end carbons is consistent with exclusive initial primary C–H bond activation for demethanation, while dihydrogen loss can result from either initial primary or secondary insertion. In addition, the observed 2:1 ratio of CD_3H to CH_3D eliminated in the reaction

(51) Schultz, R. H.; Armentrout, P. B. *J. Am. Chem. Soc.* **1991**, *113*, 729.
(52) Blomberg, M. R. A.; Siegbahn, P. E. M.; Nagashima, U.; Wennerberg, J. *J. Am. Chem. Soc.* **1991**, *113*, 424.
(53) von Helden, G.; Kemper, P. R.; Hsu, M.-T.; Bowers, M. T. *J. Chem. Phys.* **1992**, *96*, 6591.

of Ni^+ and Fe^+ with $CH_3CH_2CD_3$ implies that initial C–H insertion is substantially more facile than initial C–D insertion. The tendency to enhance demethanation over dehydrogenation by deuterating the central carbon is again consistent with both initial primary and secondary C–H bond activation for dehydrogenation but only primary C–H bond activation for methane loss.

The CH_4/H_2 branching ratios for Co^+, Ni^+, and Fe^+ reacting with C_3H_8 are 0.29, 4.0, and 2.8, respectively. As mentioned earlier, we believe that the relative energies of the H–H and C–H coupling transition states for H_2 and CH_4 elimination, denoted as $[X]^*$ and $[Y]^*$ in Figure 8, are influential in determining the CH_4/H_2 branching ratio. In addition, conservation of angular momentum effects favors CH_4 loss (due to the large decrease in reduced mass of the $MC_3H_6^+ + H_2$ product channel compared to the reactants). Consequently, for Fe^+ and Ni^+ reacting with C_3H_8, the C–H reductive coupling transition state for CH_4 elimination, $[Y]^*$, must be lower in energy than the H–H reductive coupling transition state for H_2 elimination, $[X]^*$, while for Co^+ reacting with C_3H_8, transition state $[X]^*$ is probably lower in energy than transition state $[Y]^*$. As kinetic energy is increased in the Co^+ system, the CH_4/H_2 branching ratio increases to a value more comparable to those observed for Ni^+ and Fe^+. This probably reflects the decreasing importance of the relative energies of $[X]^*$ and $[Y]^*$ in determining the branching ratio.

D. Excited Electronic States. State-selected reactivity studies[5,17,20,54] have shown that both the rate of adduct formation and H_2 and CH_4 elimination channels for Fe^+, Co^+, and Ni^+ reacting with propane are strongly dependent on the electronic configuration of the metal ion. In the metastable kinetic energy release measurements, the metal ions were formed by electron impact on $Fe(CO)_5$ and $Ni(CO)_6$. Because electron impact produces a mixture of ground and excited electronic states,[55–57] the possible effects of excited electronic states on the metastable decomposition processes must be considered.

For Ni^+, the ^2D ground state has a $3d^9$ electronic configuration, and the ^4F and ^2F, first and second excited states, have $4s3d^8$ electronic configurations.[16] State-selected rate constant measurements[54] indicate that the ^2D, $3d^9$ ground state of Ni^+ forms the $Ni(C_3H_8)^+$ adduct much more efficiently than the ^4F and ^2F, $4s3d^8$ excited states of Ni^+. The repulsive interaction of states having an occupied 4s orbital with propane reduces the lifetime of the excited-state adducts, leading to decomposition prior to the magnetic sector. As a result, metastable decomposition of electronically excited $Ni(C_3H_8)^+$ complexes is unimportant in the second field-free region.

For Fe^+, the ^6D ground state has a $4s3d^6$ electronic configuration, and the ^4F and ^4D, first and second excited states, have $3d^7$ and $4s3d^6$ electronic configurations, respectively.[16] As observed for the 4s occupied states of Ni^+, state-selected rate constant measurements[17] indicate that the lifetime of the $Fe^+(^4D, 4s3d^6)$-C_3H_8 complex is too short to contribute significantly to the metastable decomposition observed in the second field-free region. In contrast, the adduct lifetime for the ^6D, $4s3d^6$ ground state of Fe^+ is long despite the presence of a 4s electron. We believe that this is due to a crossing from the ground-state surface to the $Fe^+(^4F,3d^7)C_3H_8$ excited-state surface, where the adduct is more strongly bound.[17] The schematic reaction coordinate diagrams shown in Figure 7 and 8 depict the surface crossing. Such a crossing is consistent with ab initio calculations by Perry and Goddard[39] which indicate that for the $Fe(C_3H_8)^+$ complex the ^4E state is more stable than the ^6E state. Because the C–H bond activation transition state, which is common to reactants starting on both the ground- and the excited-state asymptotic surfaces, lies 0.075 eV below the asymptotic energy of the ^6D ground state of Fe^+, it lies 0.325 eV below the $Fe^+(^4F)/C_3H_8$ reactant energy. Consequently, $Fe(C_3H_8)^+$ complexes originating from $Fe^+(^4F)$ will be relatively short lived and will react prior to mass analysis by the magnet. In addition, if the $Fe^+(^4F)$ state contributed significantly to the $Fe(C_3H_8)^+$ decomposition, a relatively broad or bimodal KERD for CH_4 loss would be observed because the available energy from this state is 0.25 eV greater than that from the ^6D ground state. However, a narrow, unimodal, statistical KERD is observed for CH_4 elimination. Hence, the metastable reactions we observe originate primarily from ground-state $Fe^+(^6D)$ ions.

It is interesting to note that for ground-state Fe^+ reacting with propane, the reaction efficiency is observed to decrease slowly with increasing energy from 0.02 to 0.2 eV, whereas the efficiency for ground-state Ni^+ reacting with propane is observed to be constant over this energy range (hence the cross sections decrease as expected for ion–molecule collisions). Our phase space calculations predict the reaction efficiency to be essentially constant with increasing energy for both Fe^+ and Ni^+ reacting with propane. The discrepancy between theory and experiment for the Fe^+ system can be explained by noting that $Fe^+(^6D)$ reacts with propane by crossing to the quartet surface evolving from the $Fe^+(^4F)$ + propane reactants. The energy dependence associated with making this surface crossing cannot be calculated in a straightforward fashion, but its empirical characterization has been discussed elsewhere.[5]

E. Location of the C–H and C–C Bond Activation Transition States. It is interesting to compare the locations of the C–H bond activation transition states for the Fe^+/C_3H_8, Co^+/C_3H_8, and Ni^+/C_3H_8 systems. For Co^+ and Ni^+, the ground electronic configurations are $3d^8$ and $3d^9$, respectively. The C–H bond activation transition states are located 0.11 and 0.10 eV below the $Co^+(^3F,3d^8)/C_3H_8$ and $Ni^+(^2D,3d^9)/C_3H_8$ reactant energies. For Fe^+, the C–H bond activation transition state is located 0.325 eV below the $Fe^+(^4F,3d^7)/C_3H_8$ reactant energy. Because the attractive forces between propane and $Fe^+(^4F,3d^7)$, $Co^+(^3F,3d^8)$, and $Ni^+(^2D,3d^9)$ should be similar, it seems curious that the C–H bond activation transition state for $Fe^+(^4F,3d^7)$ is so much lower than that for $Co^+(^3F,3d^8)$ and $Ni^+(^2D,3d^9)$. As the metal ion inserts into the C–H bond, electron density is donated from the bonding C–H σ orbital into the empty 4s orbital of the metal ion.[19] The 4s orbital is most accessible for Fe^+, less accessible for Co^+, and even less accessible for Ni^+, as indicated by the energy differences between the states that have $3d^n$ and $4s3d^{n-1}$ configurations, as noted above. This difference is also reflected in the relative strengths of the metal–alkyl and metal–hydride bonds, where Fe^+ makes the strongest bonds, followed by cobalt, and then by nickel.[58] The relative stability of the C–H bond activation transition state should also be influenced by the interactions between the 3d electrons and the antibonding orbital of the C–H bond being broken, but this effect is difficult to quantify.

An important point to consider is that the promotion energies for forming two covalent bonds to $Fe^+(^6D)$, $Co^+(^3F)$, and $Ni^+(^2D)$ ground-state ions are nearly the same.[49] As a result, the energies of the inserted $HMC_3H_7^+$ intermediates for M = Fe, Co, and Ni are expected to be very similar. This, of course, rationalizes why the energies of the C–H bond activation transition states leading to these intermediates, ΔE^*, are found experimentally to be similar.

Evidence has been presented that strongly suggests that C–C bond activation does not occur at low energy for ground-state Fe^+ reacting with propane. As discussed earlier, threshold collisional activation experiments[51] as well as ab initio calcula-

(54) van Koppen, P. A. M.; Kemper, P. R.; Bowers, M. T., unpublished data.
(55) (a) Kemper, P. R.; Bowers, M. T. *J. Phys. Chem.* **1991**, *95*, 5134; (b) *J. Am. Chem. Soc.* **1990**, *112*, 3231.
(56) Strobel, F.; Ridge, D. P. *J. Phys. Chem.* **1989**, *93*, 3635.
(57) Oriedo, J. V. B.; Russell, D. H. *J. Phys. Chem.* **1992**, *96*, 5314.
(58) Armentrout, P. B.; Clemmer, D. E. In *Energetics of Organometallic Species*; Simoes, J. A. M., Ed.; Kluwer: the Netherlands, 1992; pp 321–356.

tions[33,52] indicate that the C–C bond activation transition state is ≥8 kcal/mol higher in energy than the C–H bond activation transition state. Because the C–H bond activation transition state is located 0.075 eV (1.7 kcal/mol) below the ground-state $Fe^+(^6D)/C_3H_8$ reactant energy, the C–C bond activation transition state should be located near or somewhat above the first excited-state $Fe^+(^4F)/C_3H_8$ reactant energy (as shown in Figure 7), a result that is consistent with threshold collisional activation experiments.[51] The relative locations of the C–H and C–C transition states are not obvious in the bimolecular reactivity of Fe^+ at higher kinetic energies, for reasons that are not presently understood.

Conclusions

Detailed information regarding the mechanism and energetics of Fe^+ and Ni^+ reacting with propane has been obtained by measuring the reaction cross sections, branching ratios, and kinetic energy release distributions for isotopically labeled and unlabeled propanes and comparing these results to predictions of statistical phase space theory.

The observed low reaction efficiencies and the significant decrease in the reaction cross section for deuterated propanes indicate that a rate-limiting transition state associated with C–H bond activation exists somewhere along the reaction coordinate. Further, the effect of deuteration on the dehydrogenation/demethanation branching ratios requires initial C–H bond activation (rather than the β-H shift after initial C–C bond activation) to be the rate-limiting transition state for demethanation and initial primary and initial secondary C–H bond activation to be rate limiting for dehydrogenation. Arguments are made that indicate that the CH_4 reductive elimination transition states are most likely not rate limiting in these systems.

For dehydrogenation, initial primary and initial secondary C–H bond activation give rise to the low- and high-energy components in the bimodal KERDs, respectively. This bimodality was observed for Fe^+, Co^+, and Ni^+ reacting with propane. The high-energy, nonstatistical component in the KERD for dehydrogenation is attributed to a barrier in the region of the exit channel. A concerted H_2 elimination mechanism has been proposed to be responsible for this barrier. The low-energy, statistical component in the KERD for dehydrogenation indicates a smooth transition to products in the exit channel, as would be expected for H_2 elimination from the dihydride intermediate proposed in Scheme 1.

For demethanation, the barrier associated with the initial insertion of the metal ion into a primary C–H bond of propane restricts the total angular momentum available to the products, reducing the high-energy portion of the product KERD. Because the KERD is very sensitive to the energy of the C–H bond activation transition state, a lower limit to the barrier height is obtained by modeling the experimental distribution using statistical phase space theory. Modeling the cross section, the isotope effect, and the KERD for CH_4 loss using statistical phase space theory indicates that the barrier for C–H bond insertion is located 0.10 ± 0.01 eV below the Ni^+/C_3H_8 asymptotic energy and 0.075 ± 0.01 eV below the Fe^+/C_3H_8 asymptotic energy.

$Fe^+(^6D)$, $Co^+(^3F)$, and $Ni^+(^2D)$ are observed to react very similarly with propane, even though the ground electronic configuration of Fe^+ is a $4s3d^6$, whereas the ground electronic configurations for Co^+ and Ni^+ are $3d^8$ and $3d^9$, respectively. The occupation of the 4s orbital in $Fe^+(^6D)$ leads to a more repulsive interaction with propane and a more weakly bound adduct than the $3d^n$ states of Co^+ and Ni^+. However, in the case of Fe^+, a crossing occurs from the ground-state $Fe^+(^6D, 4s3d^6)C_3H_8$ surface to the low-lying first excited-state $Fe^+(^4F,3d^7)C_3H_8$ surface,[5,17,20] yielding the similarity in reactivity with Co^+ and Ni^+.

Acknowledgment. The support of the National Science Foundation under Grants CHE92-19752 (M.T.B.) and CHE92-21241 (P.B.A.) is gratefully acknowledged. In addition, we gratefully acknowledge useful discussions with Jason Perry and appreciate the sharing of his work prior to publication.

Appendix

The model for statistical phase space calculations, applied to organometallic systems, has been previously outlined.[59] In these calculations, the kinetic energy distribution of product ions was obtained for comparison with experiment. In all instances the collision complex was formed through an orbiting transition state and dissociated to products via an orbiting transition state. Here we extend the calculations to include the effect of coupled transition states along the reaction coordinate on the KERDs and on reaction cross sections. This model was initially applied to reactions of Co^+ with propane and propane-d_8. Here we apply this model to reactions of Fe^+ and Ni^+ with propane and propane-d_8. The potential energy surface used in the calculations is shown in Figure 1. Competition occurs for the $M(propane)^+$ complex between dissociation back to reactants (via the orbiting transition state) and to products via a tight transition state. For $Co^+(^3F)$ and $Ni^+(^2D)$ reacting with propane, this model is quite reasonable because both systems remain on the ground-state triplet and doublet surfaces, respectively. For $Fe^+(^6D)$, however, reaction with propane is believed to involve a crossing to the quartet surface,[5,17,20] evolving from $Fe^+(^4F)$, prior to C–H bond activation (as discussed in the introduction to this paper). The simplified potential energy surface shown in Figure 1 is applicable to the Fe^+/propane system as long as initial C–H bond activation rather than surface crossing is rate limiting. In this limit, both the KERD and the relative efficiency, $\gamma(C_3H_8)/\gamma(C_3D_8)$, where $\gamma = k_{products}/k_{collision}$, will be independent of the efficiency of the surface crossing.

The probability of an $M(propane)^+$ complex with energy, E, and angular momentum, J, forming products in channel i is given by expression A1:

$$P_i(E,J) = \frac{F_i^*(E,J)}{F^{orb}(E,J) + F_i^*(E,J)} \tag{A1}$$

where $F^{orb}(E,J)$ is the microcanonical flux through the orbiting transition state back to reactants and $F_i^*(E,J)$ is the flux through the tight transition state to go on to products in channel i. Averaging over the E,J distribution resulting from a M^+ + propane collision, the probability for forming products in channel i with translational energy E_t is given by A2:

$$P(E_t) = \frac{\int_0^\infty dE\, e^{-E/kT} \int_0^{J_{max}} dJ\, 2JF_{in}^{orb}(E,J)P_i(E,J)P_i(E,J;E_t)}{\int_0^\infty dE\, e^{-E/kT} \int_0^{J_{max}} dJ\, 2JF_{in}^{orb}(E,J)} \tag{A2}$$

where $F_{in}^{orb}(E,J)$ is the flux through the orbiting transition state to form the collision complex $M(C_3H_8)^+$ and $P_i(E,J;E_t)$ is the fraction of molecules at energy E and angular momentum J decaying through the orbiting transition state to yield products i with translational energy E_t.

The bimolecular rate constant for formation of product i, $k_i(E,J)$ is given by A3:

(59) (a) van Koppen, P. A. M.; Jacobson, D. B.; Illies, A. J.; Bowers, M. T.; Hanratty, M. A.; Beauchamp, J. L. *J. Am. Chem. Soc.* **1989**, *111*, 1991. (b) Hanratty, M. A.; Beauchamp, J. L.; Illies, A. J.; van Koppen, P. A. M.; Bowers, M. T. *J. Am. Chem. Soc.* **1988**, *110*, 1. (c) van Koppen, P. A. M.; Bowers, M. T.; Beauchamp, J. L.; Dearden, D. V. In *Bonding Energetics in Organometallic Compounds*; Mark, T. J., Ed.; ACS Symposium Series 428; American Chemical Society: Washington, DC, 1990.

$$k_i(E,J) = F_{in}^{orb}(E,J)\left[\frac{F_i^{\ddagger}(E,J)}{F^{orb}(E,J) + F_i^{\ddagger}(E,J)}\right]/\rho(E,J) \quad \text{(A3)}$$

where $\rho(E,J)$ is the microcanonical density of states of the reactants. Averaging over the E,J distribution, the bimolecular rate constant relative to the total collision rate constant is

$$\frac{k_i}{k_{collision}} = \frac{\int_0^{\infty} dE\, e^{-E/kT} \int_0^{J_{max}} dJ\, 2JF_{in}^{orb}(E,J)\dfrac{F^{\ddagger}(E,J)}{F^{orb}(E,J) + F^{\ddagger}(E,J)}}{\int_0^{\infty} dE\, e^{-E/kT} \int_0^{J_{max}} dJ\, 2JF_{in}^{orb}(E,J)} \quad \text{(A4)}$$

If more than one product is formed, then

$$\frac{k_{tot}}{k_{collision}} = \frac{\sum_i k_i}{k_{collision}} \quad \text{(A5)}$$

where k_{tot} is the total bimolecular rate constant for all product channels. Equation A2 is used for comparison with experimental kinetic energy release distributions, and eqs A4 and A5 are used for comparison with reaction cross section measurements.

In order to calculate the kinetic energy distributions, structures and vibrational frequencies for the various species are required. These were taken from the literature where possible or estimated from literature values of similar species.[60] The details of the kinetic energy distributions were found to vary only weakly with structure or vibrational frequencies over the entire physically reasonable range for these quantities. The cross section is very sensitive to the frequencies used for the C-H bond activation transition state. The range in frequencies, however, is relatively small because of the upper limit on $\Delta E^{\ddagger}$ determined by modeling the KERD. In addition, the range in frequencies used is consistent with recent ab initio calculations by Perry et al.[36] on $Co(C_3H_8)^+$ complexes.

The KERDs are strongly dependent on the total energy available to the dissociating complex and hence in our model to the ΔH° of reaction. For the systems studied here, all heats of formation of products and reactants were well known, including the M(propene)$^+$ and M(ethylene)$^+$ organometallic product ions, which have been fairly well established.[59,61,62] These heats of formation were consistently used throughout the calculations and are summarized along with the parameters in Table 7.

(60) (a) Shimanouchi, T. *Table of Molecular Vibrational Frequencies Consolidated*, Vol. I.; National Bureau of Standards: Washington, DC, 1972. (b) Sverdlov, L. M.; Kovner, M. A.; Krainov, E. P. *Vibrational Spectra of Polyatomic Molecules*; Wiley: New York, 1970.

(61) Sodupe, M.; Bauschlicher, C. W., Jr.; Langhoff, S. R.; Partridge, H. *J. Phys. Chem.* **1992**, *96*, 2118.

(62) Schultz, R. H.; Armentrout, P. B., work in progress.